

Provided for non-commercial research and education use.
Not for reproduction, distribution or commercial use.



This article appeared in a journal published by Elsevier. The attached copy is furnished to the author for internal non-commercial research and education use, including for instruction at the authors institution and sharing with colleagues.

Other uses, including reproduction and distribution, or selling or licensing copies, or posting to personal, institutional or third party websites are prohibited.

In most cases authors are permitted to post their version of the article (e.g. in Word or Tex form) to their personal website or institutional repository. Authors requiring further information regarding Elsevier's archiving and manuscript policies are encouraged to visit:

<http://www.elsevier.com/copyright>



Solar activity dependence of total electron content derived from GPS observations over Mbarara

A.O. Adewale^{a,*}, E.O. Oyeyemi^{a,1}, J. Olwendo^{b,2}

^a Department of Physics, University of Lagos, Nigeria

^b Department of Physics, Pwani University College, Kenya

Received 30 December 2011; received in revised form 5 May 2012; accepted 5 May 2012

Available online 14 May 2012

Abstract

Vertical total electron content (*VTEC*) observed at Mbarara (geographic co-ordinates: 0.60°S, 30.74°E; geomagnetic coordinates: 10.22°S, 102.36°E), Uganda, for the period 2001–2009 have been used to study the diurnal, seasonal and solar activity variations. The daily values of the 10.7 cm radio flux ($F_{10.7}$) and sunspot number (R) were used to represent Solar Extreme Ultraviolet Variability (EUV). *VTEC* is generally higher during high solar activity period for all the seasons and increases from 0600 h LT and reaches its maximum value within 1400 h–1500 h LT. All analysed linear and quadratic fits demonstrate positive *VTEC*– $F_{10.7}$ and positive *VTEC*– R correlation, with all fits at 0000 h and 1400 h LT being significant with a confidence level of 95% when both linear and quadratic models are used. All the fits at 0600 h LT are insignificant with a confidence level of 95%. Generally, over Mbarara, quadratic fit shows that *VTEC* saturates during all seasons for $F_{10.7}$ more than 200 units and R more than 150 units. The result of this study can be used to improve the International Reference Ionosphere (IRI) prediction of TEC around the equatorial region of the African sector.

© 2012 COSPAR. Published by Elsevier Ltd. All rights reserved.

Keywords: Total electron content; Solar flux; Sunspot number; Equatorial region

1. Introduction

The Solar Extreme Ultraviolet Variability (EUV) and X-ray radiations provide the primary energy sources for producing plasma in the Earth's upper atmosphere. These radiations show definitive variations. Consequently, the total electron content (TEC) of the ionosphere is also expected to reflect these variations (Huang and Cheng, 1995; Chakraborty et al., 1999; Liu and Chen, 2009; Chen et al., 2009). TEC is the total number of electrons present along any path between the ground stations and Global Positioning Satellite (GPS) satellites, with units of electrons per square meter, where 10^{16} electrons/m² = 1 TEC unit

(TECU). A number of researchers have reported significant changes in the key ionospheric F-layer parameters as a result of solar activity (Kouris et al., 1998; Gupta and Singh, 2001; Marin et al., 2001; Sethi et al., 2002; Pandey et al., 2003; Liu et al., 2004a,b; Xu et al., 2004; Bremer, 2004) and geomagnetic activity (Bremer, 1992, 1998; Mikhailov and Marin, 2000) variations. Several authors have reported the solar activity dependence of TEC at high, mid and low latitudes (Balan et al., 1993; Afraimovich et al., 2008; Chen et al., 2008). Liu and Chen (2009) observed three kinds of patterns (linearity, saturation, and amplification) in TEC versus 10.7 cm radio flux ($F_{10.7}$). The relationship between TEC and solar indices (sunspot number (R) and $F_{10.7}$) or solar EUV fluxes has been found to be roughly linear (Balan et al., 1993; Afraimovich et al., 2008) and quadratic (Chen et al., 2008, 2009; Liu and Chen, 2009).

Although, solar activity variations of TEC have been carried out at various sectors around the globe, but to the best of our knowledge, no such work has been undertaken

* Corresponding author. Tel.: +234 7031113940.

E-mail addresses: olajide3000@yahoo.com (A.O. Adewale), e_oyeyemi@yahoo.co.uk (E.O. Oyeyemi), castrajoseph@yahoo.com (J. Olwendo).

¹ Tel.: +234 8067976399.

² Tel.: +254 720990555.

around the equatorial region of the African continent and this has limited our understanding of the equatorial ionosphere over the African continent. It is essential that long-time records of TEC measurements are available to track more accurately the solar activity effects on the equatorial ionosphere. Several models (e.g. IRI (Bilitza, 2001; Bilitza and Reinisch, 2008), SLIM (Anderson et al., 1987), GCPM-2000 (Gallagher et al., 2000), and NeQuick (Nava et al., 2008)) have been developed to reproduce the dominant patterns of ionospheric parameters. The International Reference Ionosphere (IRI) is the most commonly used model. The IRI project is a joint programme of the Committee on Space Research (COSPAR) and the International Union of Radio Science (URSI) initiated in the late sixties with the aim of launching an international standard for the specification of ionospheric parameters based on available data from ground-based as well as satellite observations. IRI is an empirical ionospheric model based on experimental observations of the ionospheric plasma either by ground or in-situ measurements. IRI describes monthly averages of the electron density, electron temperature, ion composition, ion temperature, and ion drift in the current altitude range of 50–2000 km. The IRI model provides three options for the prediction of TEC, namely: IRI-2001 (Bilitza, 2001), IRI01-Corr (Bilitza, 2004) and NeQuick (Radićella and Leitinger, 2001; Coisson et al., 2006).

The accuracy of the IRI model in a specific region and/or time period depends on the availability of reliable data for the specific region and time since it is a data-based model. IRI is continually updated as new data and new modeling techniques become available and this process has resulted in several versions of IRI (Rawer et al., 1978a,b, 1981; Bilitza, 1990, 2001; Bilitza and Reinisch, 2008). Bilitza and Reinisch (2008) reported that IRI predictions are most accurate over the Northern mid-latitudes because of the generally high station density in this part of the globe. The solar activity dependence on the ionosphere and thermosphere should be considered important in questions of space weather, climatology, and ionospheric modeling.

The purpose of this research is to study the diurnal, seasonal, and solar activity dependence of GPS-TEC observed at Mbarara, Uganda (geographic co-ordinates: 0.60°S, 30.74°E; geomagnetic coordinates: 10.22°S, 102.36°E) during the period 2001–2009. The result of this study might be used to improve the IRI prediction of average TEC around the equatorial region of the African sector. Although data from more equatorial Africa stations has to be included in this kind of analysis in order to have a better conclusion on the solar activity dependence of TEC.

2. Data and method of analysis

The data used for this research were obtained from University Navstar Consortium (UNAVCO) website (www.unavco.org). The Receiver Independent Exchange (RINEX) observation files obtained from this website were processed using the GPS-TEC analysis application soft-

ware, developed by Gopi Seemala of the Institute for Scientific Research, Boston College, USA.

The software calculates slant TEC (*STEC*) using GPS observables from the observation data. The *VTEC* is derived from *STEC* by using equation:

$$VTEC = [STEC - (b_R + b_S)]/S(E) \quad (1)$$

where b_R is the interfrequency differential receiver biases and b_S the interfrequency differential satellite biases. The mapping function $S(E)$ employed is given by

$$S(E) = \frac{1}{\cos(Z)} = \left\{ 1 - \left(\frac{R_E \times \cos(E)}{R_E + h_s} \right)^2 \right\}^{-0.5} \quad (2)$$

with z = zenith angle of the satellite as seen from the observing station, R_E = radius of the Earth, E = the elevation angle in radians, and h_s = the altitude of the thin layer above the surface of the Earth (taken as 350 km).

In order to minimize the multipath effects on GPS data, an elevation cut off of 20° was used. In addition to eliminating the errors from multipath, we also removed the satellite and receiver biases from the TEC values used in this present study. The satellite and receiver bias values were obtained from the data center of Bern University, Switzerland. We have used *VTEC* measurement for March Equinox (MAREQUI) (February, March, April), June Solstice (JUNSOLS) (May, June, July), September Equinox (SEPEQUI) (August, September, October), and December Solstice (DECSOLS) (November, December, January), for the year 2001–2009. In order to minimize the possible geomagnetic effects, we rejected the *VTEC* data when the geomagnetic index $A_p > 20$.

In order to see the variations of *VTEC* during the different levels of a solar cycle, we used data from 2001 to 2002 (which is close to the peak of solar cycle 23), with an average sunspot number (R) of 111.0 and 104.1, respectively, to represent a period of high solar activity (HSA), 2004–2005 with an average sunspot number (R) of 40.4 and 29.8, respectively, to represent a period of medium solar activity (MSA) and 2008–2009 with an average sunspot number (R) of 2.8 and 3.1, respectively, to represent a period of low solar activity (LSA). We have used the daily values of R and $F_{10.7}$ from 2001 to 2009 to indicate the solar activity variability.

The following goodness of fit statistics for parametric models was evaluated:

- R-square
- Adjusted R-square
- Root mean squared error (RMSE)

R-square might increase when the number of fitted coefficients in a model is increased, although the fit may not improve. To avoid this situation, we have also used the degrees of freedom adjusted R-square statistic. A 95% confidence bounds for the fitted coefficients were also calculated.

Confidence bounds define the lower and upper values of the associated interval, and define the width of the interval. The width of the interval indicates the uncertainty in the fitted coefficients.

For any data used in this paper, values of correlation coefficient (r) > 0.5 are regarded as very significant.

We use two regression methods to study the solar activity dependence of $VTEC$ over Mbarara. The first regression method is a linear approximation to describe the relationship between the solar indices and $VTEC$:

$$VTEC(S) = A_0 + A_1S \quad (3)$$

The second regression model is the quadratic relationship between solar indices and $VTEC$:

$$VTEC(S) = A_0 + A_1S + A_2S^2 \quad (4)$$

where A_0 , A_1 and A_2 are the coefficients and S denotes $F_{10.7}$ and R .

3. Results

3.1. Diurnal and seasonal variations of $VTEC$

Figs. 1–3 show the diurnal and seasonal variations of $VTEC$ (upper quartile, median, and lower quartile) values during HSA (2001–2002), MSA (2004–2005) and LSA (2008–2009). The result shows that the median values of $VTEC$ are generally higher during HSA period for all the seasons. In all the seasons considered, $VTEC$ has lower

values during daytime compared with nighttime values. $VTEC$ generally decreases during 0000 h–0600 h LT after which it starts to increase gradually until it reaches its maximum value around mid-day, during 1400 h–1500 h LT in all the seasons. The pre-sunrise minimum is seen between 0500 h and 0600 h LT in all the seasons. In DECSOLS, MAREQUI and SEPEQUI, during HSA, a secondary maximum is found to occur around 2100 h LT.

Fig. 4 shows the diurnal plots of hourly median $VTEC$ values for the four seasons during HSA, MSA and LSA. Seasonally, $VTEC$ show a semiannual variation. The median values of daytime $VTEC$ during MAREQUI are found to be higher than those of JUNSOLS during all solar activity periods.

3.2. Relationship between $VTEC$ and solar indices

Figs. 5–7 show the mass plots of $VTEC$ against $F_{10.7}$ for three local times (0000 h, 0600 h and 1400 h), representing the local mid-night, time of pre-sunrise minimum $VTEC$ and time of maximum $VTEC$. Figs. 8–10 are the plots of $VTEC$ against R for three local times at 0000 h, 0600 h and 1400 h. Table 1 shows the correlation coefficients of $VTEC$ with $F_{10.7}$ and R . The correlation coefficients at 0000 h LT and 1400 h LT are both large, indicating that $VTEC$ is dependent on both solar variables during all the seasons. However, $VTEC$ is weakly correlated with both $F_{10.7}$ and R at 0600 h LT during all the seasons. The

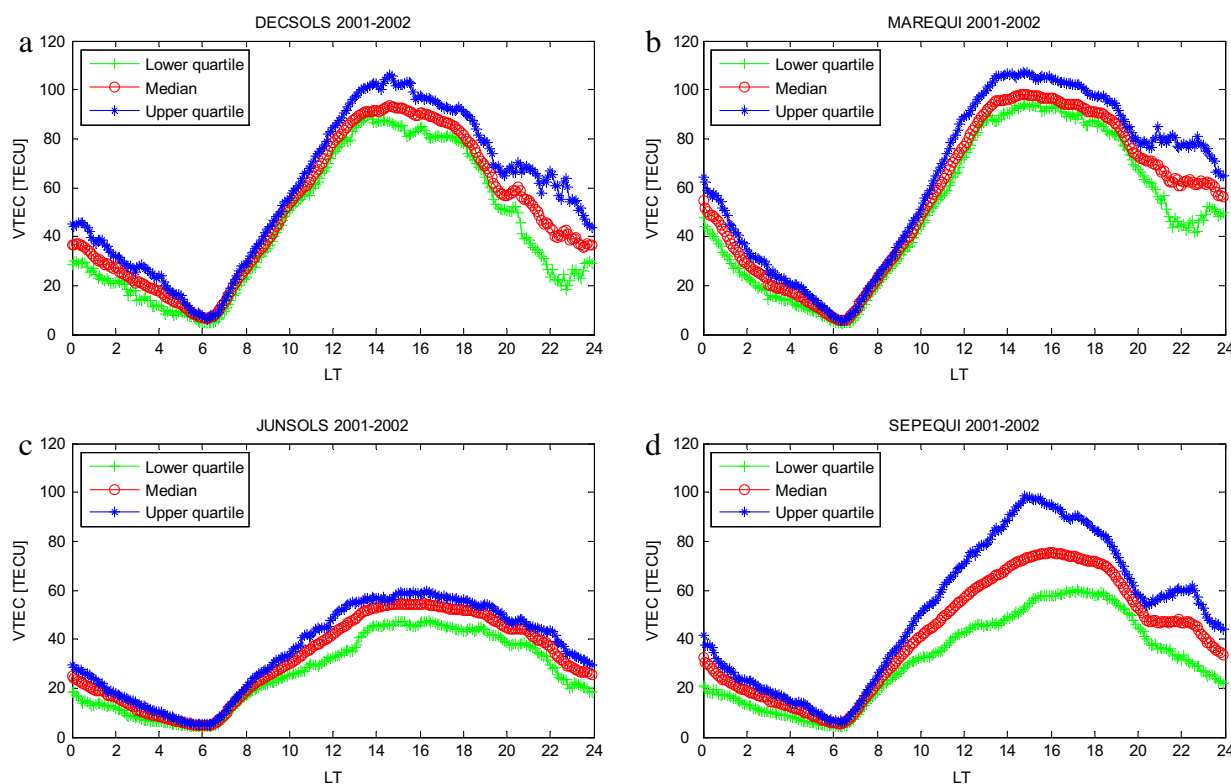


Fig. 1. Diurnal variation of median $VTEC$, Upper quartile and Lower quartile for 2001–2002.

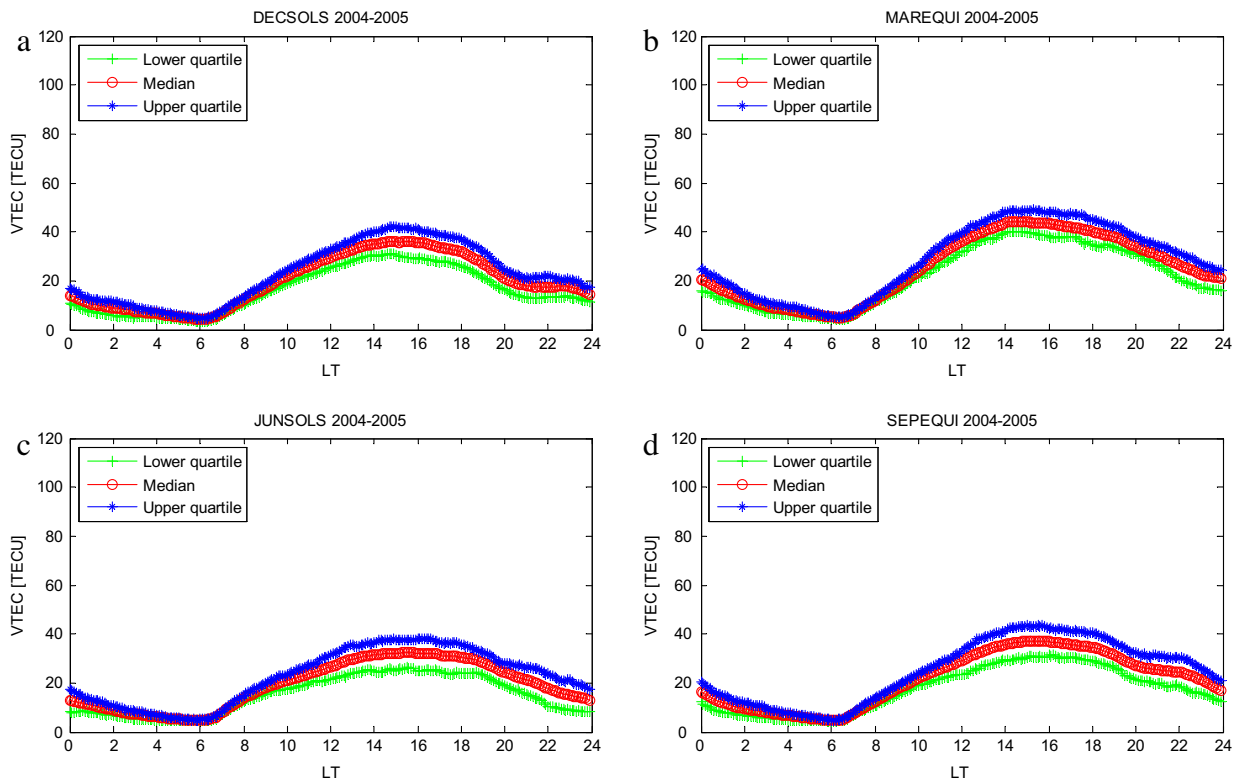


Fig. 2. Diurnal variation of median $VTEC$, Upper quartile and Lower quartile for 2004–2005.

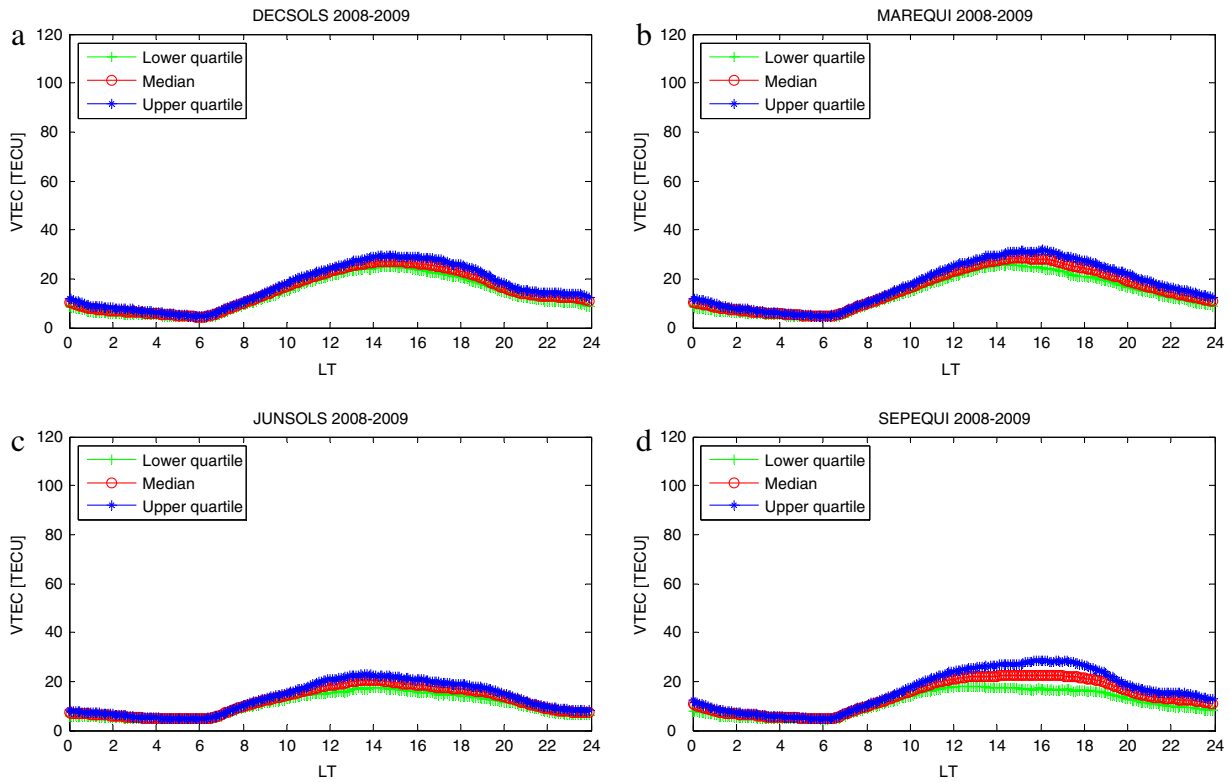


Fig. 3. Diurnal variation of median $VTEC$, Upper quartile and Lower quartile for 2008–2009.

correlation coefficients between $VTEC$ and both solar indices are insignificant (<0.4) at 0600 h LT.

We have applied a linear fittings as well as polynomial fittings of $VTEC$ versus $F_{10.7}$ and R . The result of linear

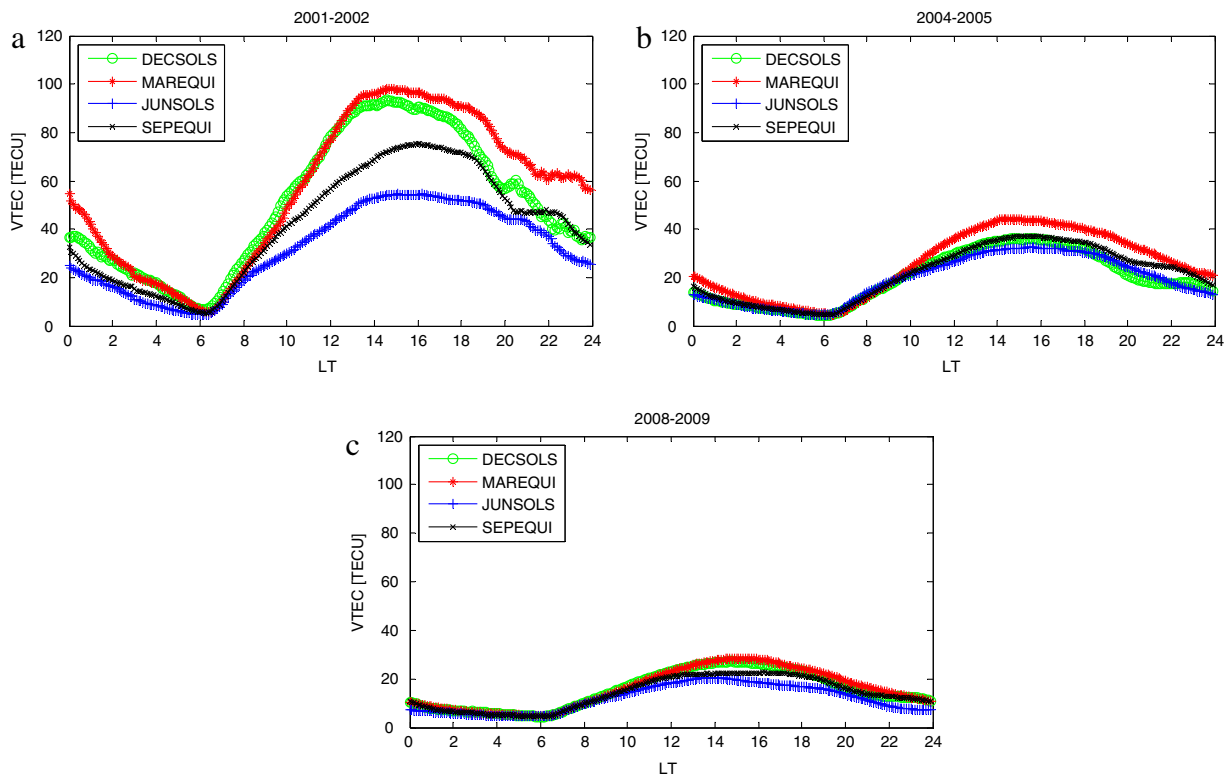


Fig. 4. Seasonal variation of VTEC for HSA, MSA and LSA.

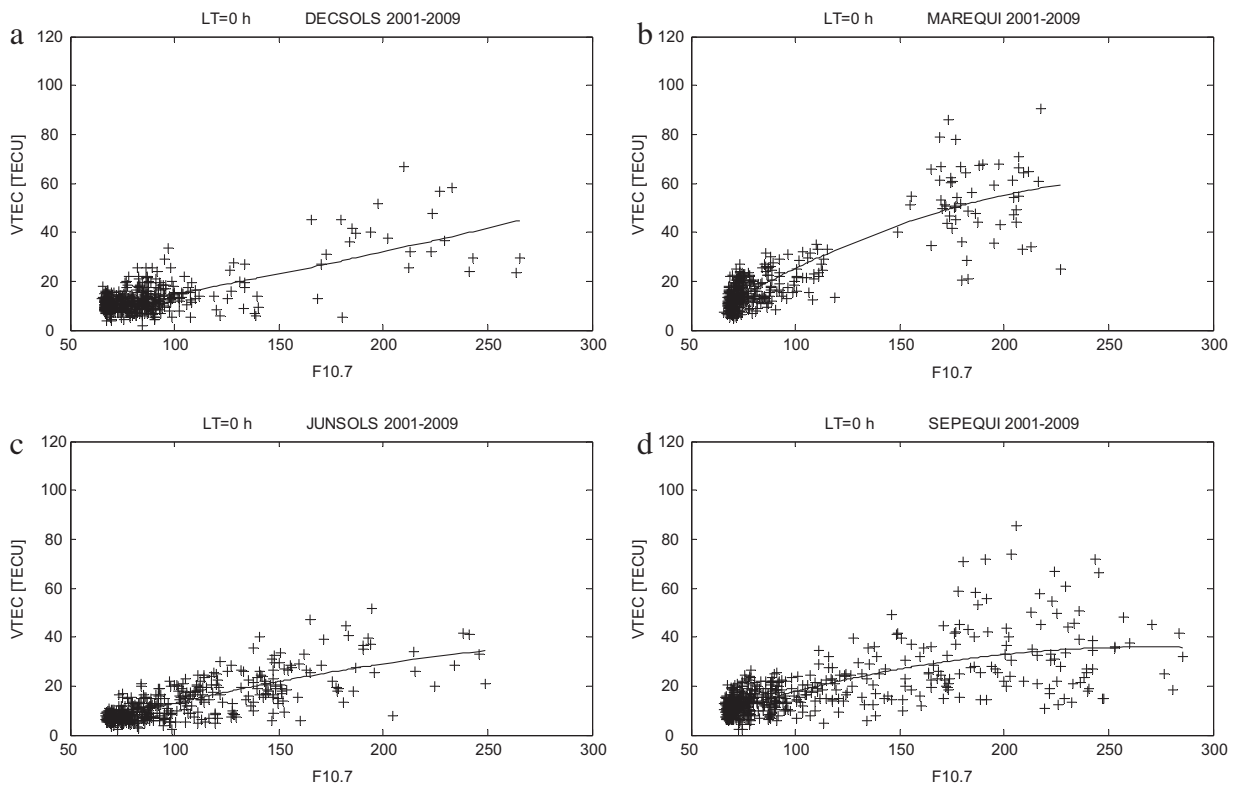


Fig. 5. Variation of $VTEC$ at 0000 h LT with solar flux ($F_{10.7}$) for DECSOLS, MAREQUI, JUNSOLS, and SEPEQUI.

and quadratic fittings analyses for the selected hours are shown in Tables 2–7. The tables show the polynomial

coefficients and the 95% confidence bounds (in brackets). The quadratic fit and the observed data are shown in Figs.

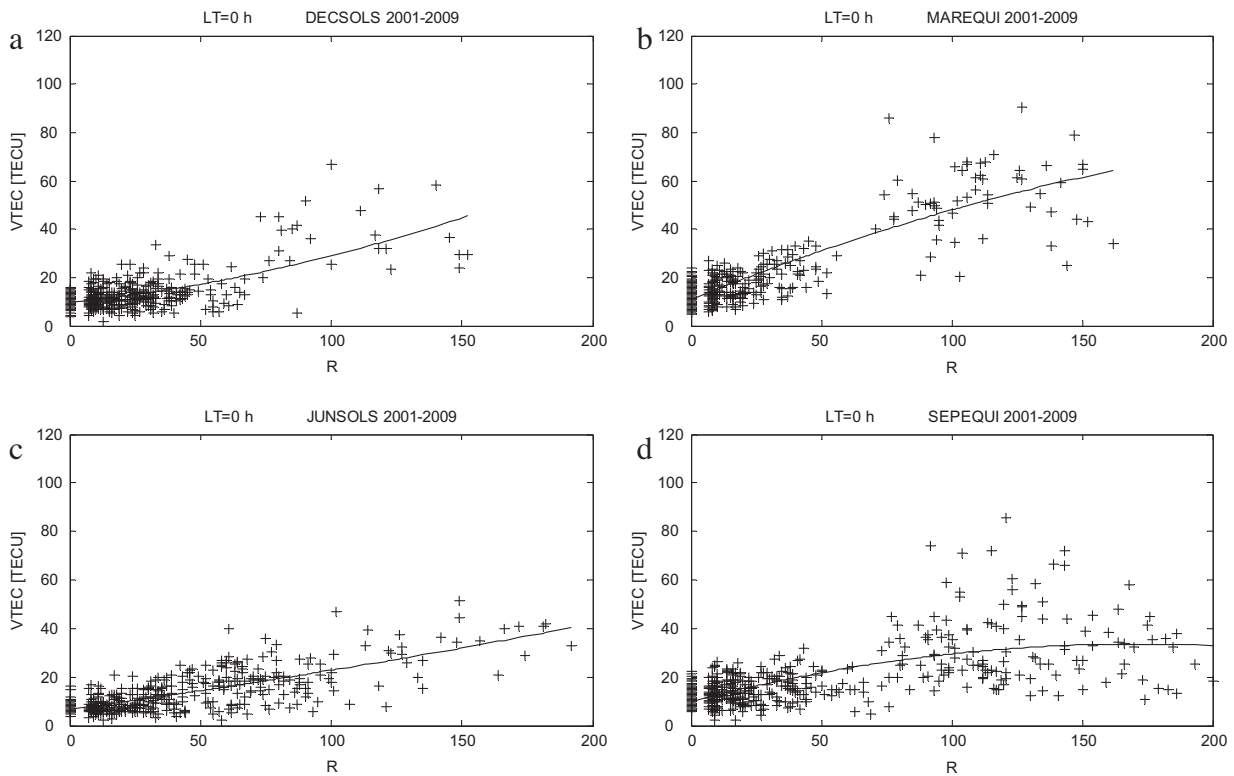


Fig. 6. Variation of $VTEC$ at 0000 h LT with sunspot number (R) for DECSOLS, MAREQUI, JUNSOLS, and SEPEQUI.

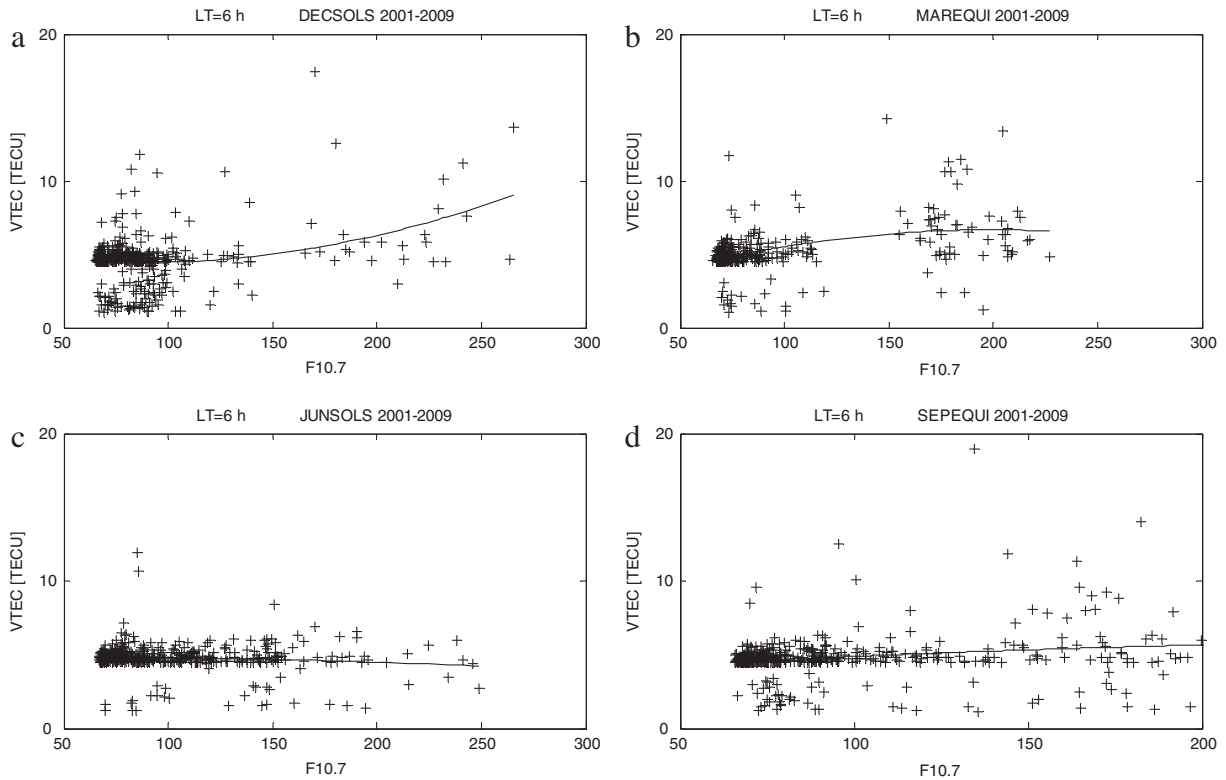


Fig. 7. Variation of $VTEC$ at 0600 h LT with solar flux ($F_{10.7}$) for DECSOLS, MAREQUI, JUNSOLS, and SEPEQUI.

5–10. The analysis of goodness of fit statistics shows that the quadratic and linear fits give similar results during all

the seasons and at all local times considered. This result shows that for application purposes, either linear or qua-

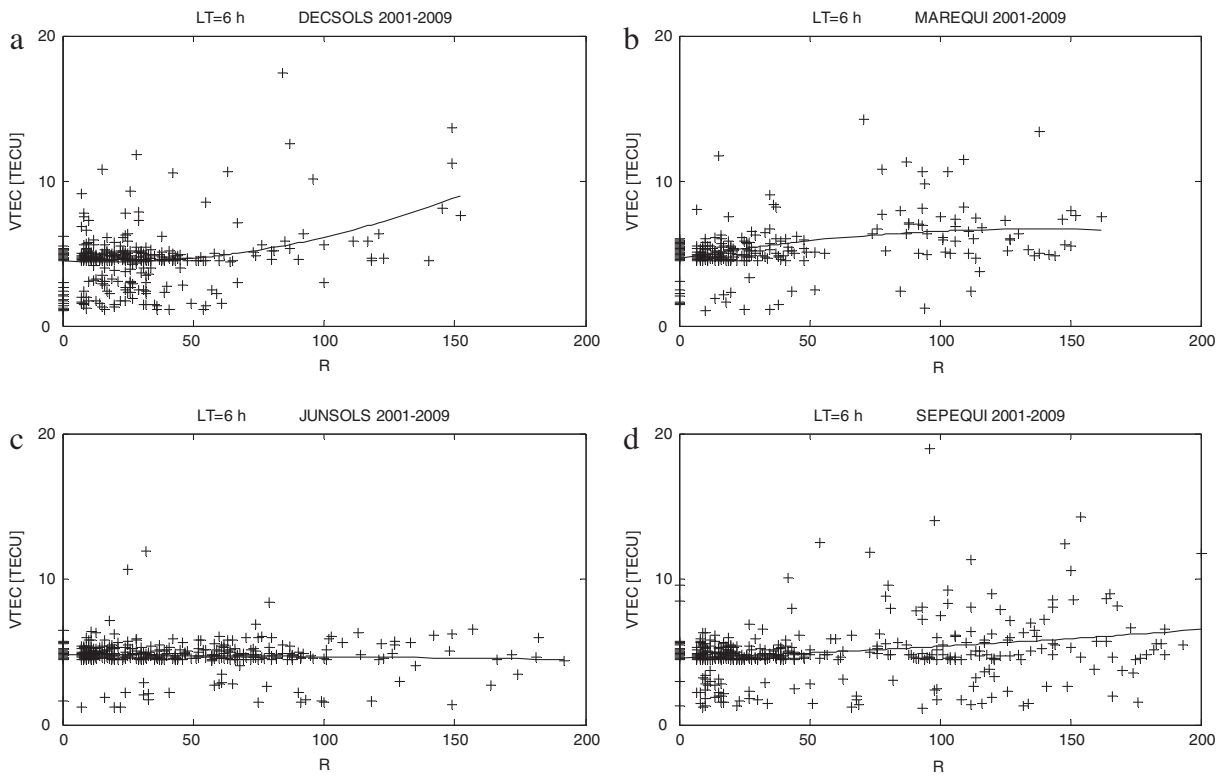


Fig. 8. Variation of $VTEC$ at 0600 h LT with sunspot number (R) for DECSOLS, MAREQUI, JUNOLS, and SEPEQUI.

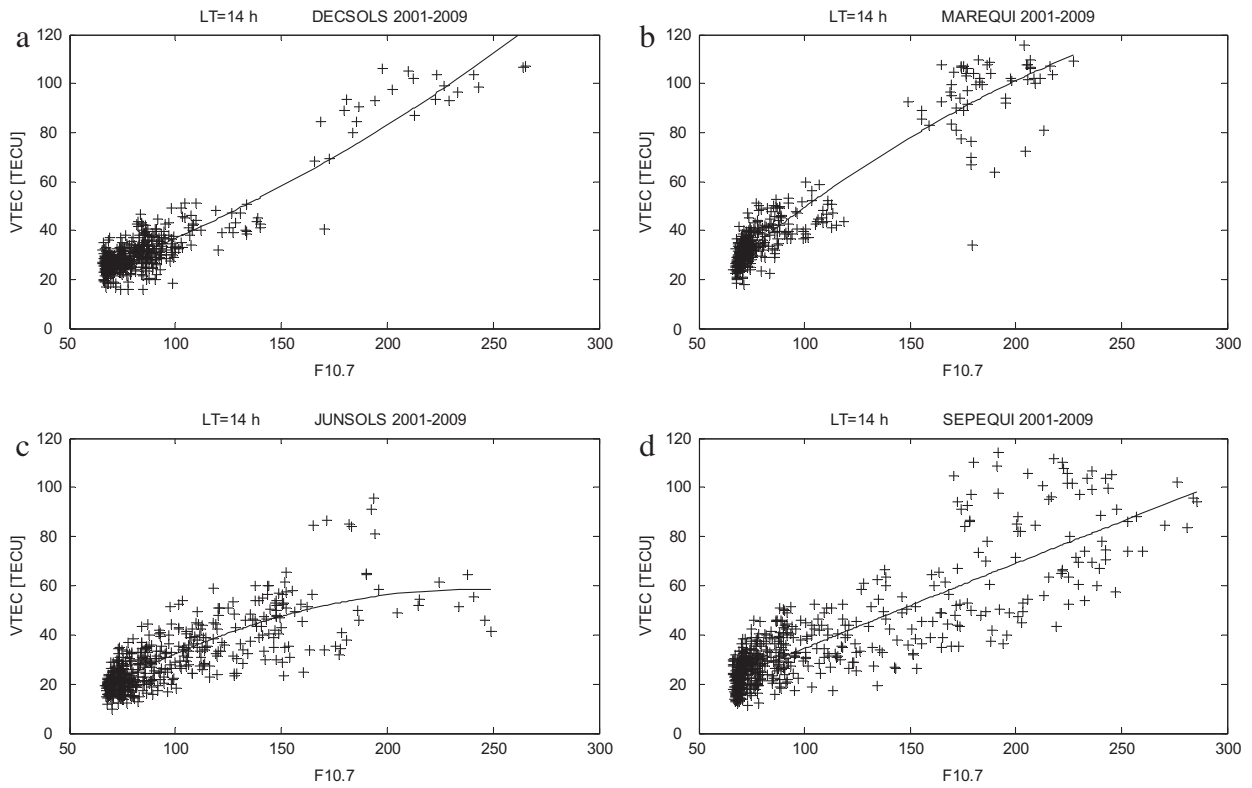


Fig. 9. Variation of $VTEC$ at 1400 h LT with solar flux ($F_{10.7}$) for DECSOLS, MAREQUI, JUNOLS, and SEPEQUI.

dratic regressions can be a good choice and higher-order regressions does not significantly improve the fitting.

Our result (Figs. 5–10) shows that there is an obvious seasonal difference in the relationship between $VTEC$ and

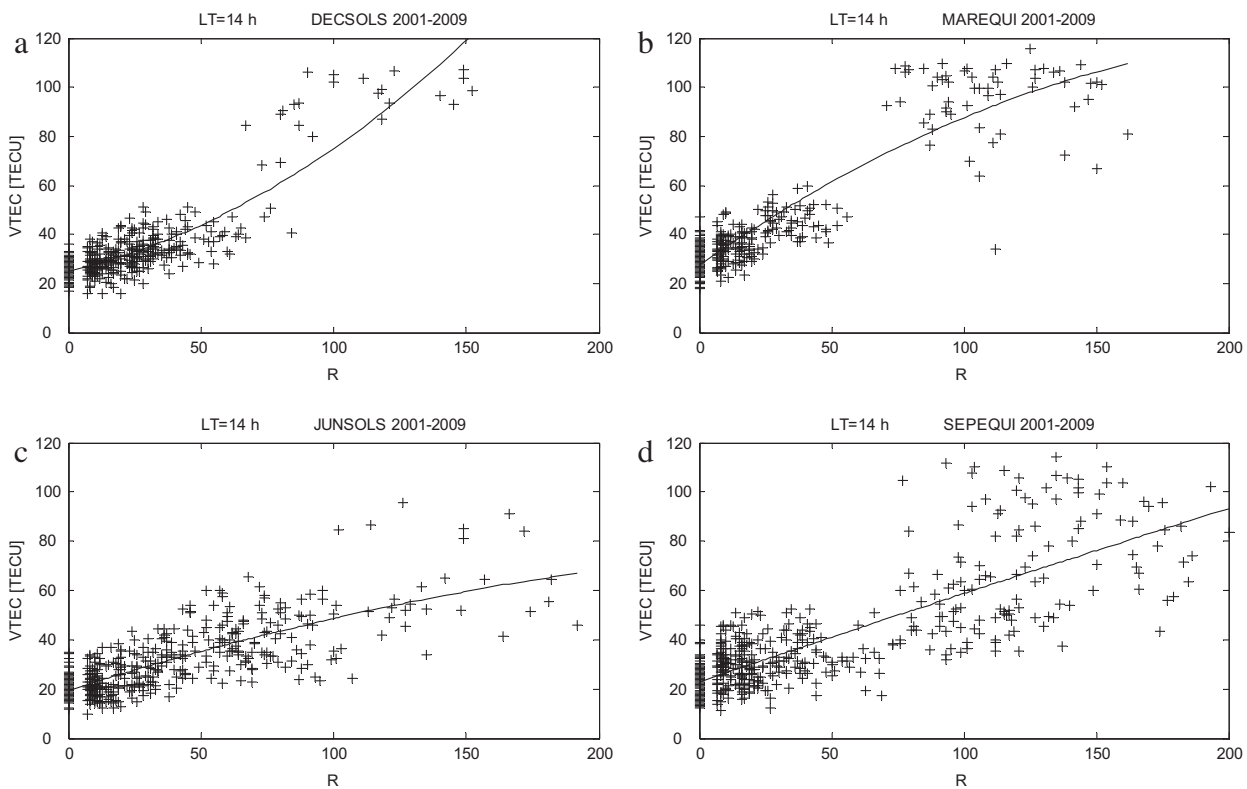


Fig. 10. Variation of *VTEC* at 1400 h LT with sunspot number (*R*) for DECSOLS, MAREQUI, JUNSOLS, and SEPEQUI.

$F_{10.7}$ (*R*). In DECSOLS (Figs. 5–10(a)), *VTEC* tends to increase with increasing solar activities. In MAREQUI, the nighttime *VTEC* increases with $F_{10.7}$ (*R*) up to about 200 flux units (150), after which *VTEC* saturates at a value of approximately 50 TECU (Figs. 5 and 6(b)), and the noontime *VTEC* increases with $F_{10.7}$ (*R*) up to about 220 flux units (150), after which *VTEC* saturates at a value approximately 100 TECU (Figs. 9 and 10(b)). The pre-sunrise *VTEC* increases with $F_{10.7}$ (*R*) up to about 150 flux units (100) and saturates at about 6 TECU (Fig. 7 and 8(b)). In JUNSOLS, the midnight *VTEC* increases very slowly with $F_{10.7}$ up to about 250 flux units (Fig. 5(c)) (however, *VTEC* tends to increase with increasing *R*, Fig. 6(c)) and noontime *VTEC* increases with $F_{10.7}$ (*R*) up to about 220 flux units (180), after which it saturates at a value approximately 60 TECU (Figs. 9 and 10(c)). The pre-sunrise *VTEC* decreases with both $F_{10.7}$ and *R* (Figs. 7 and 8(c)). In SEPEQUI, nighttime *VTEC* increases with $F_{10.7}$ (*R*) up to about 220 flux units (150), after which

VTEC saturates at a value of approximately 30 TECU (Figs. 5 and 6(d)). Noontime *VTEC* increases steadily with $F_{10.7}$ and *R* (Figs. 9 and 10(d)). Our study shows that the rate of increase of daytime *VTEC* is greatest in MAREQUI and least in JUNSOLS.

4. Discussion

We have investigated the diurnal, seasonal and solar activity variations of *VTEC* over an equatorial station. Our result shows that *VTEC* are generally higher during HSA period for all the seasons (Fig. 4). Most of the contributions to TEC come from the electron density in the *F* region. Hence both TEC and the peak electron density of the *F2* region (N_mF_2) share similar features (Gupta and Singh, 2001; Chen et al., 2009). *VTEC* are generally higher during HSA period because temperature variations cause ionospheric electron content to increase with increasing solar activity and radiation intensity and *VTEC* depends on the temperature profile in the thermosphere, and increasing solar activity raises the thermospheric temperature (Stubbe, 1964; Rishbeth, 1964).

In all the seasons considered, as shown in Fig. 4, *VTEC* has higher values during daytime compared with nighttime values. Around sunrise hours, with the beginning of intensive ionization, the electron concentration near the *F2*-peak increases at a rate which primarily depends upon the production rate. TEC values generally increases from 0600 h LT in all the seasons and reaches its maximum value during

Table 1
Correlation coefficients between solar indices and *VTEC*.

	Solar flux ($F_{10.7}$)			Sunspot number (<i>R</i>)		
	0 h LT	06 h LT	14 h LT	0 h LT	6 h LT	14 h LT
DECSOLS	0.72	0.30	0.92	0.67	0.27	0.86
MAREQUI	0.88	0.36	0.94	0.87	0.36	0.91
JUNSOLS	0.78	-0.09	0.79	0.77	-0.07	0.78
SEPEQUI	0.70	0.24	0.85	0.67	0.25	0.82

Table 2
Coefficients of the linear and quadratic fits and their corresponding goodness of fit statistics for solar flux ($F_{10.7}$) at 0h.

00h00 LT	Linear fit					Quadratic fit					
$F_{10.7}$	Coefficients (with 95% confidence bounds)		R-square	Adj R-square	RMSE	Coefficients (with 95% confidence bounds)			R-square	Adj R-square	RMSE
	A_0	A_1				A_0	A_1	A_2			
DECSOLS	-1.926 (-3.32, -0.53)	0.169 (0.154, 0.184)	0.51	0.51	5.25	0.265 (-4.26, 4.785)	0.130 (0.0526, 0.208)	0.000140 (-0.000135, 0.000416)	0.51	0.51	5.25
MAREQUI	-11.480 (-13.340, -9.618)	0.343 (0.325, 0.362)	0.77	0.77	7.47	-27.230 (-35.990, -18.470)	0.6367 (0.476, 0.798)	-0.00112 (-0.00173, -0.000512)	0.78	0.78	7.36
JUNSOLS	-5.247 (-6.580, -3.914)	0.177 (0.164, 0.189)	0.60	0.60	5.13	-10.130 (-14.050, -6.211)	0.265 (0.197, 0.333)	-0.000345 (-0.000606, -0.0000845)	0.60	0.60	5.10
SEPEQUI	0.845 (-0.705, 2.395)	0.155 (0.142, 0.168)	0.49	0.49	8.44	-9.956 (-14.680, -5.234)	0.341 (0.263, 0.418)	-0.000632 (-0.000893, -0.000370)	0.51	0.51	8.28

Table 3
Coefficients of the linear and quadratic fits and their corresponding goodness of fit statistics for sunspot number (R) at 0h.

00h00 LT	Linear fit					Quadratic fit					
R	Coefficients (with 95% confidence bounds)		R-square	Adj R-square	RMSE	Coefficients (with 95% confidence bounds)			R-square	Adj R-square	RMSE
	A_0	A_1				A_0	A_1	A_2			
DECSOLS	8.821 (8.178, 9.464)	0.195 (0.176, 0.215)	0.45	0.45	5.56	9.692 (8.933, 10.450)	0.111 (0.0641, 0.155)	0.000827 (0.000429, 0.00122)	0.47	0.47	5.47
MAREQUI	11.380 (10.480, 12.290)	0.358 (0.338, 0.378)	0.76	0.76	7.70	10.760 (9.730, 11.780)	0.443 (0.373, 0.5076)	-0.000683 (-0.00122, -0.000148)	0.76	0.76	7.64
JUNSOLS	6.485 (5.875, 7.095)	0.165 (0.153, 0.177)	0.59	0.59	5.15	6.738 (6.021, 7.454)	0.146 (0.115, 0.1764)	0.000151 (-0.0000745, 0.000377)	0.59	0.59	5.15
SEPEQUI	11.27 (10.37, 12.18)	0.159 (0.145, 0.174)	0.45	0.45	8.75	9.945 (8.922, 10.970)	0.277 (0.229, 0.324)	-0.000811 (-0.00112, -0.000501)	0.48	0.47	8.56

Table 4
Coefficients of the linear and quadratic fits and their corresponding goodness of fit statistics for solar flux ($F_{10.7}$) at 6h.

06h00 LT	Linear fit					Quadratic fit					
$F_{10.7}$	Coefficients (with 95% confidence bounds)		R-square	Adj R-square	RMSE	Coefficients (with 95% confidence bounds)			R-square	Adj R-square	RMSE
	A_0	A_1				A_0	A_1	A_2			
DECSOLS	3.217 (2.805, 3.630)	0.0154 (0.011, 0.0198)	0.09	0.09	1.58	5.454 (4.112, 6.796)	-0.0242 (-0.0473, -0.00116)	0.000142 (0.0000609, 0.000223)	0.11	0.11	1.56
MAREQUI	3.690 (3.282, 4.099)	0.0159 (0.0118, 0.0199)	0.13	0.13	1.64	2.071 (0.133, 4.008)	0.0461 (0.0106, 0.0817)	-0.000116 (-0.000251, 0.0000196)	0.14	0.13	1.64
JUNSOLS	5.017 (4.769, 5.265)	-0.00241 (-0.00476, -0.0000643)	0.01	0.01	0.92	4.794 (4.070, 5.518)	0.00158 (-0.0108, 0.0139)	-0.0000156 (-0.0000631, 0.0000319)	0.01	0.01	0.92
SEPEQUI	4.038 (3.717, 4.36)	0.00796 (0.00526, 0.0107)	0.06	0.05	1.75	3.658 (2.666, 4.650)	0.0145 (-0.00185, 0.0308)	-0.0000223 (-0.0000772, 0.0000327)	0.06	0.05	1.75

1400 h–1500 h LT. These peaks are found to be associated with smaller chemical losses at higher altitudes, in addition to the production of solar radiations during daytime (Fejer et al. 1991; Lee and Reinisch, 2006). Rishbeth and Garriott (1969) reported that the production by solar radiation and loss by chemical recombination play important roles in the formation of F2 layer. Observed TEC values show a minimum at 0600 h LT for all the seasons considered and during all solar activity periods. In the evening since the primary source of ionization is no longer present, $VTEC$ value attain a lower value than the daytime value.

For the seasonal variations in $VTEC$, the daytime values are greater in MAREQUI than during SEPEQUI while the lowest values are observed during JUNSOLS as expected. This is because the sun shines directly over the equatorial region during equinoctial months and thus leads to the strongest ionization over these regions. Hence, the maximum value of $VTEC$ is observed during MAREQUI. Our study shows that the rate of increase of daytime $VTEC$ is greatest in MAREQUI and least in JUNSOLS.

Solar activity dependence of $VTEC$ varies with local time and season, as shown in Figs. 5–10. The $VTEC$ has

Table 5
Coefficients of the linear and quadratic fits and their corresponding goodness of fit statistics for sunspot number (R) at 6h.

06h00 LT	Linear fit					Quadratic fit					
	Coefficients (with 95% confidence bounds)		R-square	Adj R-square	RMSE	Coefficients (with 95% confidence bounds)			R-square	Adj R-square	RMSE
	A_0	A_1				A_0	A_1	A_2			
DECSOLS	4.200 (4.016, 4.384)	0.0174 (0.0119, 0.0229)	0.08	0.07	1.59	4.466 (4.250, 4.682)	-0.00875 (-0.0216, 0.00414)	0.000252 (0.000139, 0.000365)	0.11	0.11	1.56
MAREQUI	4.750 (4.557, 4.943)	0.0166 (0.0123, 0.0209)	0.13	0.13	1.64	4.651 (4.431, 4.870)	0.0296 (0.0152, 0.0439)	-0.000108 (-0.000222, 0.0000635)	0.14	0.13	1.64
JUNSOLS	4.836 (4.721, 4.95)	-0.00167 (-0.00388, 0.000527)	0.01	0.01	0.92	4.833 (4.698, 4.967)	-0.00145 (-0.00705, 0.00414)	-0.00000175 (-0.00004262, 0.0000391)	0.01	0.01	0.93
SEPEQUI	4.545 (4.364, 4.726)	0.00887 (0.00601, 0.0117)	0.06	0.06	1.74	4.574 (4.366, 4.783)	0.00628 (-0.00331, 0.0159)	0.0000178 (-0.0000452, 0.0000809)	0.06	0.06	1.75

Table 6
Coefficients of the linear and quadratic fits and their corresponding goodness of fit statistics for solar flux ($F_{10.7}$) at 14h.

14h00 LT	Linear fit					Quadratic fit					
	Coefficients (with 95% confidence bounds)		R-square	Adj R-square	RMSE	Coefficients (with 95% confidence bounds)			R-square	Adj R-square	RMSE
	A_0	A_1				A_0	A_1	A_2			
DECSOLS	-5.874 (-7.430, -4.318)	0.444 (0.428, 0.461)	0.85	0.85	5.88	6.827 (1.897, 11.76)	0.218 (0.134, 0.304)	0.000813 (0.000513, 0.00111)	0.86	0.86	5.71
MAREQUI	-8.705 (-10.660, -6.750)	0.559 (0.539, 0.578)	0.89	0.89	7.89	-23.66 (-32.9, -14.43)	0.838 (0.668, 1.007)	-0.00107 (-0.00171, -0.000423)	0.89	0.89	7.80
JUNSOLS	0.522 (-1.716, 2.759)	0.299 (0.278, 0.321)	0.60	0.60	8.58	-17.97 (-24.34, -11.6)	0.633 (0.523, 0.743)	-0.00131 (-0.00173, -0.000883)	0.63	0.63	8.29
SEPEQUI	-0.210 (-2.312, 1.892)	0.346 (0.329, 0.364)	0.72	0.72	11.43	-1.023 (-7.517, 5.471)	0.360 (0.253, 0.467)	0.0000477 (-0.000408, 0.000313)	0.72	0.72	11.44

Table 7
Coefficients of the linear and quadratic fits and their corresponding goodness of fit statistics for sunspot number (R) at 14h.

14h00 LT	Linear fit					Quadratic fit					
	Coefficients (with 95% confidence bounds)		R-square	Adj R-square	RMSE	Coefficients (with 95% confidence bounds)			R-square	Adj R-square	RMSE
	A_0	A_1				A_0	A_1	A_2			
DECSOLS	22.400 (21.510, 23.300)	0.509 (0.482, 0.536)	0.74	0.74	7.74	25.060 (24.080, 26.040)	0.247 (0.188, 0.306)	0.00253 (0.00202, 0.00305)	0.79	0.78	7.08
MAREQUI	28.880 (27.730, 30.020)	0.571 (0.545, 0.596)	0.83	0.83	9.75	27.470 (26.190, 28.740)	0.754 (0.670, 0.837)	-0.00152 (-0.00219, -0.000861)	0.84	0.84	9.52
JUNSOLS	20.370 (19.340, 21.390)	0.279 (0.258, 0.299)	0.60	0.60	8.62	19.570 (18.370, 20.770)	0.338 (0.287, 0.389)	-0.000471 (-0.000847, -0.0000955)	0.61	0.60	8.57
SEPEQUI	23.000 (21.710, 24.290)	0.356 (0.336, 0.376)	0.67	0.67	12.42	22.880 (21.400, 24.370)	0.366 (0.298, 0.435)	-0.0000713 (-0.000521, 0.000378)	0.67	0.67	12.43

been found to have very good linear correlation with both $F_{10.7}$ and R during noontime and midnight periods. All analysed linear and quadratic fits demonstrate positive $VTEC-F_{10.7}$ and positive $VTEC-R$ correlation, with all fits at 0000 h and 1400 h LT being significant with a confidence level of 95% when both linear and quadratic models are used. All the fits at 0600 h LT are insignificant with a confidence level of 95%. More work still has to be carried out on the solar activity dependence on equatorial Africa VTEC. However, we can suggest that a second degree poly-

nomial relation of solar activity effect on TEC, rather than the present two-segmented linear pattern in IRI (Bilitza, 2000), can be incorporated into IRI model so as to improve the prediction of TEC around the equatorial region of the African sector for a given time and month.

5. Conclusion

This study has analyzed $VTEC$ obtained from Mbarara, Uganda (geographic co-ordinates: 0.60°S, 30.74°E; geo-

magnetic coordinates: 10.22°S, 102.36°E) during the period 2001–2009 to investigate diurnal, seasonal, and solar activity variations of GPS–TEC. In summary, the major results are outlined below:

- *VTEC* are generally higher during HSA period for all the seasons.
- *VTEC* has higher values during daytime compared with nighttime values. TEC values generally increases from 0600 h LT in all the seasons and reaches its maximum value during 1400 h–1500 h LT.
- Daytime values of *VTEC* are greater in MAREQUI than during SEPEQUI while the lowest values are observed during JUNSOLS. Our study shows that the rate of increase of daytime *VTEC* is greatest in MAREQUI and least in JUNSOLS.
- Solar activity dependence of *VTEC* varies with local time and season. Our result shows that a quadratic fit can statistically describe the solar activity dependence of TEC for application purposes. Hence we recommend the application of a quadratic function in describing the solar activity effects of TEC in IRI model. This might improve IRI prediction.

Acknowledgement

The authors would like to thank the University Navstar Consortium (UNAVCO) for allowing access to their website. UNAVCO is a non-profit membership-governed consortium that facilitates geoscience research and education using geodesy. The authors would also like to thank Dr Gopi Seemala of the Institute for Scientific Research, Boston College, USA for providing access to the GPS TEC analysis software.

References

- Anderson, D.N., Mendillo, M., Herniter, B. A semi-empirical low-latitude ionospheric model. *Radio Sci.* 22, 292–306, 1987.
- Afraimovich, E.L., Astafyeva, E.I., Oinats, A.V., Yasukevich, Y.V., Zhivetiev, I.V. Global electron content: a new conception to track solar activity. *Ann. Geophys.* 26, 335–344, 2008.
- Balan, N., Bailey, G.J., Jayachandran, B. Ionospheric evidence for a nonlinear relationship between the solar E.U.V. and 10.7 cm fluxes during an intense solar cycle. *Planet. Space Sci.* 41 (2), 141–145, [http://dx.doi.org/10.1016/0032-0633\(93\)90043-2](http://dx.doi.org/10.1016/0032-0633(93)90043-2), 1993.
- Bilitza, D. A correction for the IRI topside electron density model based on Alouette/ISIS topside sounder data. *Adv. Space Res.* 33 (6), 838–843, 2004.
- Bilitza, D. (Ed.). *International Reference Ionosphere 1990*, NSSDC 90-22, Greenbelt, Maryland, 1990.
- Bilitza, D. *International Reference Ionosphere 2000*. *Radio Sci.* 36 (2), 261–275, 2001.
- Bilitza, D. The importance of EUV indices for the International Reference Ionosphere. *Phys. Chem. Earth* 25 (5–6), 515–521, 2000.
- Bilitza, D., Reinisch, B.W. *International Reference Ionosphere 2007: improvements and new parameters*. *Adv. Space Res.* 42, 599–609, 2008.
- Bremer, J. Ionospheric trends in mid-latitudes as a possible indicator of the atmospheric greenhouse effect. *J. Atmos. Terr. Phys.* 54, 1505–1511, 1992.
- Bremer, J. Investigations of long-term trends in the ionosphere with world-wide ionosonde observations. *Adv. Radio Sci.* 2, 253–258, 2004.
- Bremer, J. Trends in the ionospheric E and F region over Europe. *Ann. Geophys.* 16, 989–996, 1998.
- Chakraborty, S.K., DasGupta, A., Ray, S., Banerjee, S. Long-term observations of VHF scintillation and total electron content near the crest of the equatorial anomaly in the Indian longitude zone. *Radio Sci.* 34, 241–255, 1999.
- Chen, Y., Liu, L., Wan, W., Yue, X., Su, S. Solar activity dependence of the topside ionosphere at low latitudes. *J. Geophys. Res.* 114, A08306, <http://dx.doi.org/10.1029/2008JA013957>, 2009.
- Chen, Y., Liu, L., Le, H. Solar activity variations of nighttime ionospheric peak electron density. *J. Geophys. Res.* 113, A11306, <http://dx.doi.org/10.1029/2008JA013114>, 2008.
- Coisson, P., Radicella, S.M., Leitinger, R., Nava, B. Topside electron density in IRI and NeQuick: features and limitations. *Adv. Space Res.* 37, 937–942, 2006.
- Fejer, B.G., de Paula, E.R., Gonzales, S.A., Woodman, R.F. Average vertical and zonal plasma drift over Jicamarca. *J. Geophys. Res.* 96, 13901–13906, 1991.
- Gallagher, D.L., Craven, P.D., Comfort, R.H. Global core plasma model. *J. Geophys. Res.* 105 (A8), 18819–18833, 2000.
- Gupta, J.K., Singh, L. Long term ionospheric electron content variations over Delhi. *Ann. Geophys.* 18, 1635–1644, <http://dx.doi.org/10.1007/s00585-001-1635-8>, 2001.
- Huang, Y., Cheng, K. Solar cycle variation of the total electron content around equatorial anomaly region in East Asia. *J. Atmos. Terr. Phys.* 57 (12), 1503–1511, 1995.
- Kouris, S.S., Bradley, P.A., Dominici, P. Solar-cycle variation of the daily *f*_oF2 and M(3000)F2. *Ann. Geophys.* 16, 1039–1042, 1998.
- Lee, C.C., Reinisch, B.W. Quiet-condition hmF2, NmF2 and B0 variations at Jicamarca and comparisons with IRI-2001 during solar maximum. *J. Atmos. Sol.-Terr. Phys.* 68, 2138–2146, 2006.
- Liu, L., Chen, Y. Statistical analysis of solar activity variations of total electron content derived at Jet Propulsion Laboratory from GPS observations. *J. Geophys. Res.* 114, A10311, <http://dx.doi.org/10.1029/2009JA014533>, 2009.
- Liu, L., Wan, W., Ning, B. Statistical modeling of ionospheric foF2 over Wuhan. *Radio Sci.* 39, RS2013, <http://dx.doi.org/10.1029/2003RS003005>, 2004a.
- Liu, L., Luan, X., Wan, W., Lei, J., Ning, B. Solar activity variations of equivalent winds derived from global ionosonde data. *J. Geophys. Res.* 109, A12305, <http://dx.doi.org/10.1029/2004JA010574>, 2004b.
- Marin, D., Mikhailov, A.V., de la Morena, B.A., Herraiz, M. Long-term hmF2 trends in the Eurasian longitudinal sector from the ground-based ionosonde observations. *Ann. Geophys.* 19, 761–772, 2001.
- Mikhailov, A.V., Marin, D. Geomagnetic control of the foF2 long-term trends. *Ann. Geophys.* 18, 653–665, 2000.
- Nava, B., Coisson, P., Radicella, S.M. A new version of the NeQuick ionosphere electron density model. *J. Atmos. Sol.-Terr. Phys.* 70, 1856–1862, 2008.
- Pandey, V.K., Sethi, N.K., Mahajan, K.K. Dependence of F2-peak height on solar activity: a study with incoherent scatter measurements. *Adv. Space Res.* 31 (3), 543–548, [http://dx.doi.org/10.1016/S0273-1177\(03\)00049-8](http://dx.doi.org/10.1016/S0273-1177(03)00049-8), 2003.
- Radicella, S.M., Leitinger, R. The evolution of the DGR approach to model electron density profiles. *Adv. Space Res.* 27 (1), 35–40, 2001.
- Rawer, K., Bilitza, D., Ramakrishnan, S. Goals and status of the International Reference Ionosphere. *Rev. Geophys.* 16, 177–181, 1978a.
- Rawer, K., Ramakrishnan, S., Bilitza, D. *International Reference Ionosphere*, International Union of Radio Science, URSI Special Report. Bruxelles 75, 1978.

- Rawer, K., Lincoln, J.V., Conkright, R.O. International Reference Ionosphere IRI-79, world data center A for solar-terrestrial physics, Report UAG-82. Boulder, Colorado, 1981.
- Rishbeth, H. A time-varying model of the ionospheric F2-layer. *J. Atmos. Terr. Phys.* 26, 657–685, 1964.
- Rishbeth, H., Garriott, O.K. Introduction to Ionospheric Physics. Academic Press, New York, pp. 98–108, 1969.
- Sethi, N.K., Goel, M.K., Mahajan, K.K. Solar cycle variations of foF2 from IGY to 1990. *Ann. Geophys.* 20, 1677–1685, 2002.
- Stubbe, P. Temperature variation at the F-layer maximum during a sunspot cycle. *J. Atmos. Terr. Phys.* 26, 1055–1068, 1964.
- Xu, Z.-W., Wu, J., Igarashi, K., Kato, H., Wu, Z.-S. Long-term ionospheric trends based on ground-based ionosonde observations at Kokubunji, Japan. *J. Geophys. Res.* 109, A09307, <http://dx.doi.org/10.1029/2004JA010572>, 2004.